# Aggregated Modeling and Power Hardware-in-the-Loop Emulation of Grid Impedance

Henrik Alenius*, Tuomas Messo
Laboratory of Electrical Energy Engineering
*Tampere University of Technology*
Tampere, Finland
*henrik.alenius@tut.fi

Tommi Reinikka, Tomi Roinila
Laboratory of Automation and Hydraulics
*Tampere University of Technology*
Tampere, Finland

***Abstract*—The rapid growth of renewable energy production increases the number of grid-connected inverters in the power system. The interface between the inverter and the grid may face stability issues, which can be assessed using impedance-based stability criterion. The frequency-dependent grid impedance is often an unknown parameter, and vastly simplified grid impedance models are widely used. Most common modeling approach is to use series-connected inductor as the grid impedance. However, measurements on real grids have shown the grid to be more complex, resonant, and time-variant. This paper introduces a grid-impedance model based on aggregation of sub-models, which drastically simplifies complex grid modeling, while still accurately captures resonances and possible time-variant behavior. Numerical sensitivity analysis is carried out for grid parameters to illustrate the significance of separate grid elements. Lastly, impedance measurements are shown for emulated full-order and aggregated impedance models in an experimental power hardware-in-the-loop setup.**

## I. Introduction

The access to reliable and affordable energy is vital for a modern society. The share of renewable distributed generation (DG) has grown exponentially at the expense of conventional fossil fuels, and thus the penetration of grid-connected inverters is increasing at a rapid pace [1]. The dynamics of power-electronic interface are complex and power quality problems or even instability have been reported in utility-scale wind and solar power plants [2]–[4].

Impedance-based stability analysis has been used to predict harmonic resonances and stability-issues at the grid-converter interface [5]. The analysis is based on the ratio of converter output impedance to grid impedance at the point-of-common coupling (PCC), and therefore the impact of grid impedance on the operation of grid-connected converters have been considered in many publications [6]–[14]. Traditional power system analysis provides accurate information on the grid impedance at the fundamental frequency. However, the frequency-dependent grid impedance is often unknown and typically modeled as a series inductance [15], sometimes combined with series resistance. Measurements on real power grids have shown the grid impedance to be more complex, resonant, and time-variant [16]–[20]. In low-voltage (LV) grids, measurements have shown parallel resonances in the frequency range of 250 to 750 Hz in the grid impedance [21], [22]. The resonant behavior in LV grids origins from the capacitive elements present in consumer loads, i.e. grid-side filter capacitances in electronics [23], cables, or reactive power compensators. Thus, common models for the grid impedance in the stability assessment of grid-connected converters are often inadequate and overly simplified [16], [24]. Modeling the grid impedance more realistically would improve the accuracy of stability analysis. Weak grids impose challenging operating conditions for grid-connected converters, as sufficient impedance-based stability margins are more difficult to reach. In addition, possible stability issues may be overlooked when the weak grid is depicted solely through short-circuit ratio (SCR) or inductance value. Therefore, the dynamics of grid impedance outside fundamental frequency and possible grid resonances should be considered when assessing the stability of the converter-grid interface.

This work presents a method for enhanced grid-impedance modeling by aggregating the model significantly, while still accurately addressing the resonant and time-variant characteristics of the grid impedance. The method is based on sub-model approach where the similar grid elements are aggregated in order to reduce system complexity while still including the key-elements. In addition, sensitivity analysis is performed by varying parameter values for better understanding of parameter impact on the shape of grid impedance. Finally, a power hardware-in-the-loop (PHIL) system for testing of grid-connected three-phase inverter in varying grid impedance condition is presented. The grid impedance models are simulated in a real-time digital simulator (RTDS), which determines the reference voltages of a three-phase linear amplifier. A test-inverter is connected to the virtual grid emulated by the linear amplifier. Thus, real hardware can be connected to emulated grid impedance, making the test system highly versatile.

The remainder of the paper is organized as follows; Section II discusses the fundamental theory related to modeling and measuring the grid impedance. In Section III, a full-order grid impedance model is shown and aggregated using the presented method. Section IV presents the sensitivity analysis of grid parameters. Section V shows the experimental PHIL setup and the experimental results of the impedance measurements from the grid emulation. Finally, Section VI concludes the main findings and discusses guidelines for modeling of the grid impedance for stability assessment of grid-connected devices.

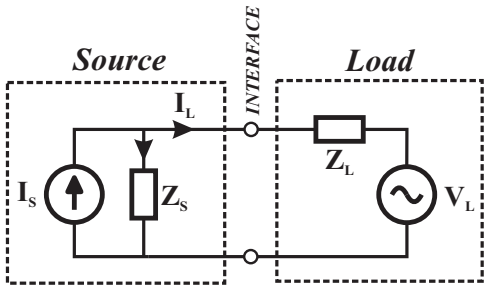


Fig. 1. Equivalent source-load model for stability assessment of inverter-grid interface.

## II. Grid Impedance Characteristics

### A. Impedance-based stability

Impedance-based stability criterion was first applied for power-electronic interfaces in [5]. The criterion is based on Kirchhoff's equations of the source-load interface, where the source is depicted as Norton equivalent and the load as Thevenin equivalent, as shown in Fig. 1. The equation for load current is

$$I_{\mathrm{L}} = \left(I_{\mathrm{S}} - \frac{V_{\mathrm{L}}}{Z_{\mathrm{S}}}\right) * \left(\frac{1}{1+\frac{Z_{\mathrm{L}}}{Z_{\mathrm{S}}}}\right) \tag{1}$$

where $I_{\mathrm{S}}$ and $Z_{\mathrm{S}}$ are source current and impedance, and $V_{\mathrm{L}}$ and $Z_{\mathrm{L}}$ are load voltage and impedance, respectively. When both systems are internally stable, the stability depends on the latter term in the equation, which resembles the transfer function of a negative feedback system in closed loop. Thus, the stability can be assessed based on Nyquist stability criterion.

### B. Definition of weak grid

A weak grid refers to a part of the grid where the impedance of the transmission system is relatively large, i.e. the load currents have major impact on the grid voltages. The precise definition of the weak grid varies in the literature, as the weakness of the grid depends on the application, and is always relative. The most common way to define a weak grid is low short-circuit ratio (SCR) value, given by

$$\mathrm{SCR} = \frac{S_{\mathrm{sc}}}{S_{\mathrm{n}}} = \frac{U_{\mathrm{g}}^2}{Z_{\mathrm{g}} S_{\mathrm{n}}}, \tag{2}$$

where $S_{\mathrm{sc}}$ is the short-circuit apparent power, $S_{\mathrm{n}}$ the nominal apparent power, $U_{\mathrm{g}}$ nominal grid voltage, and $Z_{\mathrm{g}}$ the equivalent grid impedance at fundamental frequency. However, SCR values for weak grid are incoherent, ranging from 2.5 to 10 [9], [25]–[27]. In large distributed or HVDC systems, the SCR values can be even lower ranging from 1 to 2.5, and such grids can be considered as *ultra weak grids* [28]–[30].

Another common way to describe a weak system in power electronics is through a large equivalent grid inductance value, often within 1…5 mH [8], [31]–[33]. However, these values are often arbitrary and chosen for the sake of demonstrating methods for control or interaction mitigation.

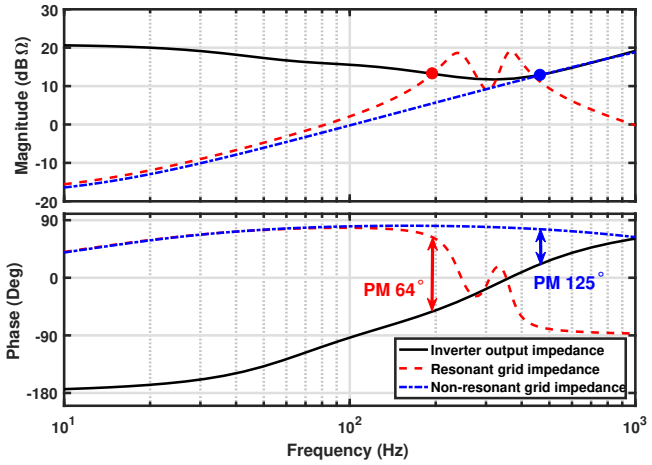


Fig. 2. Bode diagram of q-channel inverter output impedance in comparison with resonant and non-resonant grid impedance.

### C. Resonant and time-variant grid impedance

The grid impedance is often modeled as a series resistance and inductance of a few mH at a low voltage PCC [15]. This simplified approach models the impact of long transmission line on grid impedance adequately, as the lines and transformers are mainly inductive. However, the approach completely neglects the effect of capacitive elements, loads, and distributed generation. Parasitic capacitances are present in all electric systems, and many appliances introduce significant capacitive elements to system. The equivalent capacitance from multiple parallel capacitances is given by $C_{eq} = \Sigma C$, and consequently, capacitances may add up to a large equivalent value. Especially a local low voltage distribution system usually has significant equivalent capacitance [21]. As the high-voltage upstream grid is usually mainly inductive, the parallel connection with capacitive distribution system forms a parallel LC-resonance to the grid impedance seen from the PCC. The resonant frequency is given by

$$f_{\mathrm{res}} = \frac{1}{2\pi\sqrt{C_{\mathrm{eq}} L_{\mathrm{eq}}}} \tag{3}$$

and it can be as low as 250 Hz in some systems [21]. The parallel resistance resulting from passive loads in the system damps the resonance, and therefore the resonance has the greatest impact when the power consumption is at the lowest value.

Fig. 2 illustrates the impact of parallel resonance in the grid impedance, which significantly reduces the system stability margins. The output impedance of a 10 kVA three-phase inverter is compared with two grid impedances. The grid impedances consist of simple, RL-type upstream connection, but the resonant grid has an additional capacitive parallel component. With the use of simplified models, the capacitive component is neglected and stability assessment may overlook the possible issues around resonant frequency. In this case,

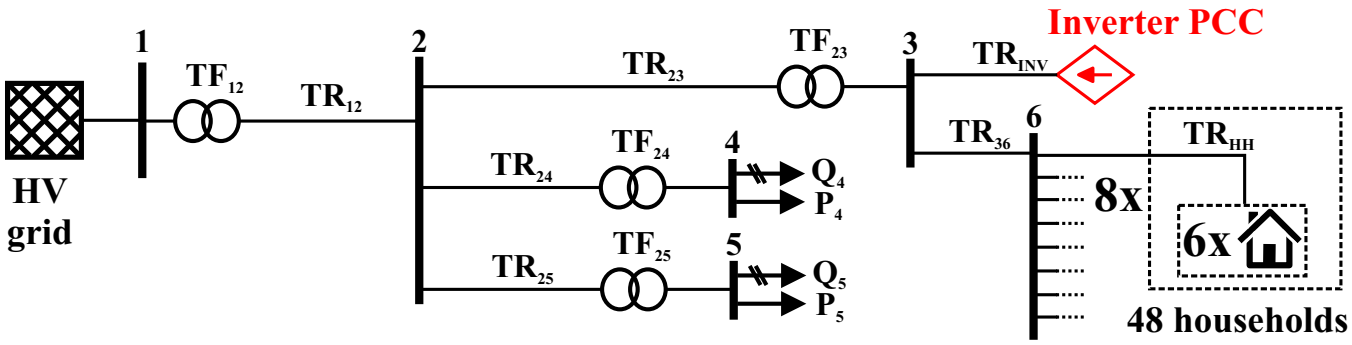


Fig. 3. Complete grid connection of an inverter to an LV distribution grid.

the grid resonance reduces the impedance-based phase margin from 125 to 64 degrees.

As the power of consumer loads is highly time variant, the resulting equivalent resistance may experience drastic changes based on the time of the day. Consequently, the magnitude of resonant behavior in the grid is fluctuating and may have unpredicted impact on the impedance-based stability margins. In the grid-impedance measurements carried out in [17], the grid impedance magnitude increased by 200 % at a resonant frequency during nighttime due to decreased damping of the increased parallel resistance. With the widely used RL-model for grid impedance, the time-variance is neglected. However, even the inclusion of variance does not adequately describe the behavior of the grid impedance, as the resonant grid is significantly more sensitive to parameter variance than a series RL-model.

### D. Measuring grid impedance

Due to high complexity of the power grid, grid impedance measurements are often required at the PCC for accurate stability assessment. The grid impedance corresponds to a transfer function from current to voltage, and thus, the grid impedance is usually extracted by injecting an excitation current to a system and measuring the resulting voltage perturbation [34], [35]. The grid impedance is simply the ratio of measured voltage to measured current in frequency-domain. In order to obtain accurate impedance measurement over a wide frequency range, the energy of the current injection should be evenly distributed, and ideally controllable. [36] Consequently, measurements based on impulse responses or passive methods often result in inadequate signal-to-noise ratio at some frequencies [37]. In this work, a sine-sweep is used to inject a sinusoidal perturbation at separate frequencies, thus providing accurate results with the highest achievable signal-to-noise ratio.

## III. Modeling grid impedance

Although the grid impedance is an important parameter for stability assessment of converters, no unified methods exist for accurate modeling. Complete models of complex grids are usually unpractical and calculation-intense, and on the other hand the widely adopted series RL-model may be too inaccurate. This section presents a method for enhanced grid impedance modeling, which aggregates the significant elements of grid impedance to a concise presentation, while still keeping the model relatively simple.

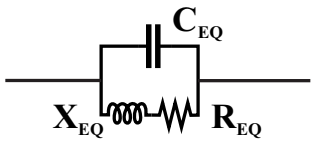


Fig. 4. Equivalent impedance of a household.

### A. Aggregation of sub-models

The separate grid entities can be considered as sub-models, which are an effective tool for modeling complex grids. The most important sub-models are upstream grid, distribution grid, and distributed generation. Upstream grid consists of the connection to stiff high-voltage grid, which is assumed to have a very high short-circuit ratio [38]. The main elements of this connection are transmission lines and transformers, so a resistive-inductive sub-model describes upstream branch with a high accuracy. Distribution grid refers to a low voltage system usually consisting of household customer cluster. The impedance of a household can be modeled as in Fig. 4, where $C_{\mathrm{EQ}}$, $R_{\mathrm{EQ}}$ and $X_{\mathrm{EQ}}$ are the equivalent capacitance, resistance and reactance, respectively [22]. The adjacent households are aggregated into a single similar model. The equivalent capacitance of an average household varies from 0.5 to 6 $\mu$F [21], or even up to 12 $\mu$F [23]. The equivalent resistance is approximated from the power consumption based on $R_{EQ} = U^2 * P_{\mathrm{tot}}^{-1}$ and correspondingly, the reactance is $X_{EQ} = R_{\mathrm{EQ}} \sqrt{\frac{1}{\mathrm{PF}^2} - 1}$. In order to accurately aggregate distribution systems into simple impedance models, the following assumptions should be adequately met

- households are relatively close to each other
- bulk of the consumption is from resistive loads (i.e. heating)
- stray capacitances can be considered additive.

### B. Complete grid-impedance model

Fig. 3 presents the impedance model for the connection of photovoltaic (PV) plant near low-voltage consumer center. The grid impedance at the PCC of the PV inverter is analyzed. The inverter connects to node 3 through transmission line $TR_{INV}$. Table I presents the system and element parameters for the full-order grid model. An LV distribution system of 48 households consists of 8 clusters of 6 households in each. Households are modeled separately (as shown in Fig. 4), with $\pm 20\%$ variance in capacitance, power consumption, and in household transmission line length.

TABLE I
PARAMETER VALUES FOR FULL-ORDER GRID IMPEDANCE MODEL.

| Parameter | Symbol | Value |
|---|---|---|
| System frequency | $\omega_s$ | $2\pi$*60 Hz |
| LV voltage | $U_L$ | 0.207 kV |
| MV voltage | $U_M$ | 10 kV |
| HV voltage | $U_H$ | 110 kV |
| Base impedance | $Z_b$ | 0.5760 Ω |
| Node 4 reactive load | $Q_4$ | 75 kVA |
| Node 4 active load | $P_4$ | 300 kW |
| Node 5 reactive load | $Q_5$ | 37.5 kVA |
| Node 5 active load | $P_5$ | 187.5 kW |
| Household consumption | $S_{HH}$ | 400...2000±20% VA |
| Household power factor | $PF_{HH}$ | $0.9...0.95_{ind}$ |
| Household capacitance | $C_{HH}$ | 4.0...6.5±20% $\mu$F |
| Number of households | $n_{HH}$ | 48 |

| Element | Resistance | Reactance |
|---|---|---|
| HV/MV transformer $TF_{12}$ | 0.000017 p.u. | j0.00017 p.u. |
| MV/LV transformer $TF_{23}$ | 0.0075 p.u. | j0.04 p.u. |
| MV/LV transformer $TF_{24}$ | 0.002 p.u. | j0.01 p.u. |
| MV/LV transformer $TF_{25}$ | 0.003 p.u. | j0.015 p.u. |
| HV line $TR_{12}$ | 0.0005 p.u. | j0.0009 p.u. |
| MV line $TR_{23}$ | 0.06 p.u. | j0.08 p.u. |
| MV line $TR_{24}$ | 0.03 p.u. | j0.05 p.u. |
| MV line $TR_{25}$ | 0.03 p.u. | j0.07 p.u. |
| LV line $TR_{36}$ | 0.139 p.u. | j0.069 p.u. |
| Line to households $TR_{HH}$ | 0.025±20% p.u. | j0.017±20% p.u. |
| Line to inverter $TR_{INV}$ | 0.069 p.u. | j0.035 p.u. |

### C. Aggregated grid-impedance model

In this section, a complex full-order grid-impedance model is greatly simplified with the use of element aggregation. Fig. 5 presents the simplified grid impedance model, where upstream grid is depicted as a series RL-impedance, and distribution system as an equivalent aggregated impedance and transmission line. Equivalent parameters for aggregated model of households are based on average values of households. In the MV grid, the other feed-in lines to different LV nodes are neglected due to significantly larger impedance than the HV connection. The order of the impedance model is drastically reduced, in this case from 112 to 5, yet the main characteristics of the grid impedance are well preserved.

The accuracy of model aggregation is verified with comparing the analytical results of the different modeling approaches.

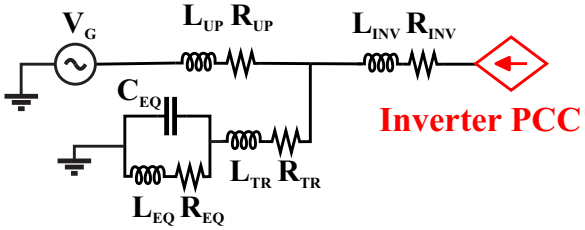


Fig. 5. Aggregated equivalent model of grid impedance.

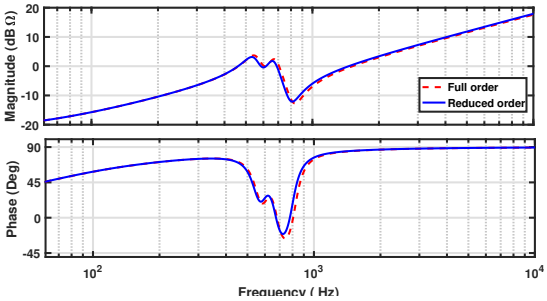


Fig. 6. Grid impedance d-component with complex and simplified model.

The grid impedance d-component $Z_{dd}$ is analytically derived from state-state representation for both models, as briefly shown for a parallel RLC-circuit in the Appendix. Fig. 6 shows the $Z_{dd}$ for full-order grid impedance and simplified impedance model. Although the impedance model is simplified, the impedances match each other very accurately. The presented method provides an effective compromise between full-order modeling and often too simple series RL-model.

TABLE II
PARAMETERS FOR AGGREGATED GRID IMPEDANCE MODEL.

| Parameter | Symbol | Value |
|---|---|---|
| **Upstream system** | | |
| Equivalent inductance | $L_{up}$ | 183.6 $\mu$F |
| Equivalent resistance | $R_{up}$ | 39.2 mΩ |
| Short-circuit -ratio | SCR | 7.2 |
| **Distribution system** | | |
| Equivalent capacitance | $C_{eq}$ | 192...312 $\mu$F |
| Equivalent resistance | $R_{eq}$ | 0.45...2.3 Ω |
| Equivalent inductance | $L_{eq}$ | 0.539...2.9 mH |
| Transmission resistance | $R_{tr}$ | 0.1 Ω |
| Transmission inductance | $L_{tr}$ | 133 $\mu$H |
| **PCC of inverter** | | |
| Transmission resistance | $R_{inv}$ | 39.7 mΩ |
| Transmission inductance | $L_{inv}$ | 53.5 $\mu$H |

## IV. IMPEDANCE SENSITIVITY TO PARAMETER CHANGES

This section describes overview of numerical sensitivity analysis of grid parameters, for illustrating the effect of separate grid elements on the resulting grid impedance. Parameter values are separately varied and the resulting grid impedance is shown for six different grid elements. The results are obtained numerically with the full-order grid impedance

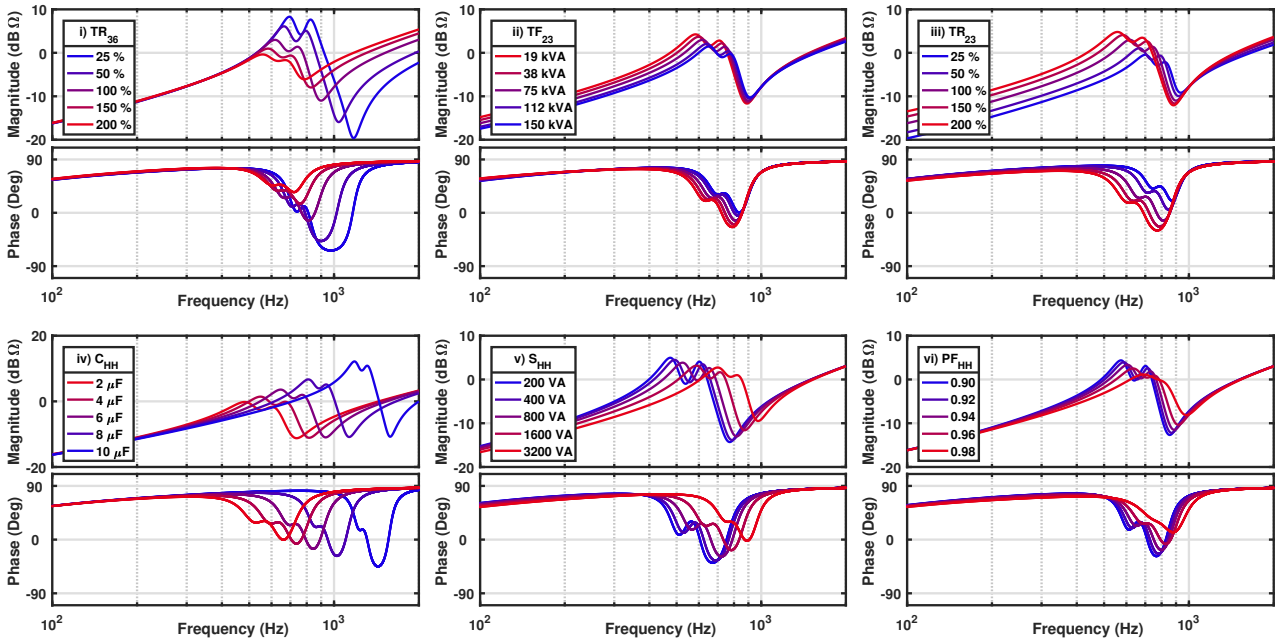


Fig. 7. Sensitivity analysis of model parameters on grid impedance.

model at the nominal state of high power consumption. Fig. 7 presents the results of this experimental sensitivity analysis. The parameters varied were

(i) transmission line length between nodes 3 and 6
(ii) transformer 23 sizing
(iii) transmission line length between nodes 2 and 3
(iv) household equivalent capacitance
(v) household apparent power consumption
(vi) household load power factor (inductive).

The most significant parameters were chosen for sensitivity analysis. The other MV branches (nodes 4 and 5) had very minimal impact on the grid impedance, as well as the HV side of the upstream grid, so they were neglected from this analysis. Therefore, the upstream impedance modeled as series RL consists of mainly transmission between LV and HV systems ($Z_{\text{TF23}}$ and $Z_{\text{TR23}}$). As the grid has a distinct main resonant frequency, variation in parameters directly related to this resonance had the greatest effect. Consequently, the capacitance of households ($C_{\text{HH}}$) and the inductance of transmission line to distribution system ($L_{\text{TF36}}$) were emphasized. The power consumption in distribution system damps the resonant behavior, and shifts the resonant frequency based on the chosen power factor for households. In addition, the figure illustrates the effects of upstream and distribution systems; the upstream system affects mainly in the frequency range below resonant frequency, and distribution system in higher frequencies.

The sensitivity analysis of the grid impedance for a system with a nearby LV distribution system can be concluded as follows

- parameters directly related to resonant characteristics are emphasized
- upstream system consists of direct transmission from stiff HV to LV grid
- distribution system affects mainly resonant behavior and in high frequencies
- upstream system affects mainly in frequencies below resonant frequency
- active power consumption in passive loads damps the resonant behavior.

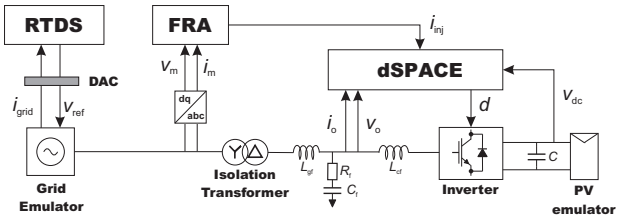


Fig. 8. PHIL setup for grid impedance emulation.

## V. Grid Impedance Emulation using PHIL-setup

The grid-impedance model is utilized in a PHIL setup capable of testing real hardware in various operating conditions [39]. This paper verifies the operation of the setup and usability of the presented grid-impedance modeling method. Fig. 8 presents the simplified test-system configuration. The grid impedance is simulated in RTDS, and is further emulated in a 4-quadrant linear grid emulator (Spitzenberger Spies PAC 15000). On the other side of the system are a three-phase inverter (Myway Plus MWINV-9R144 –inverter) and PV emulator (Spitzenberger Spies PVS 7000), which are controlled in a dSPACE real-time simulation. An isolation transformer

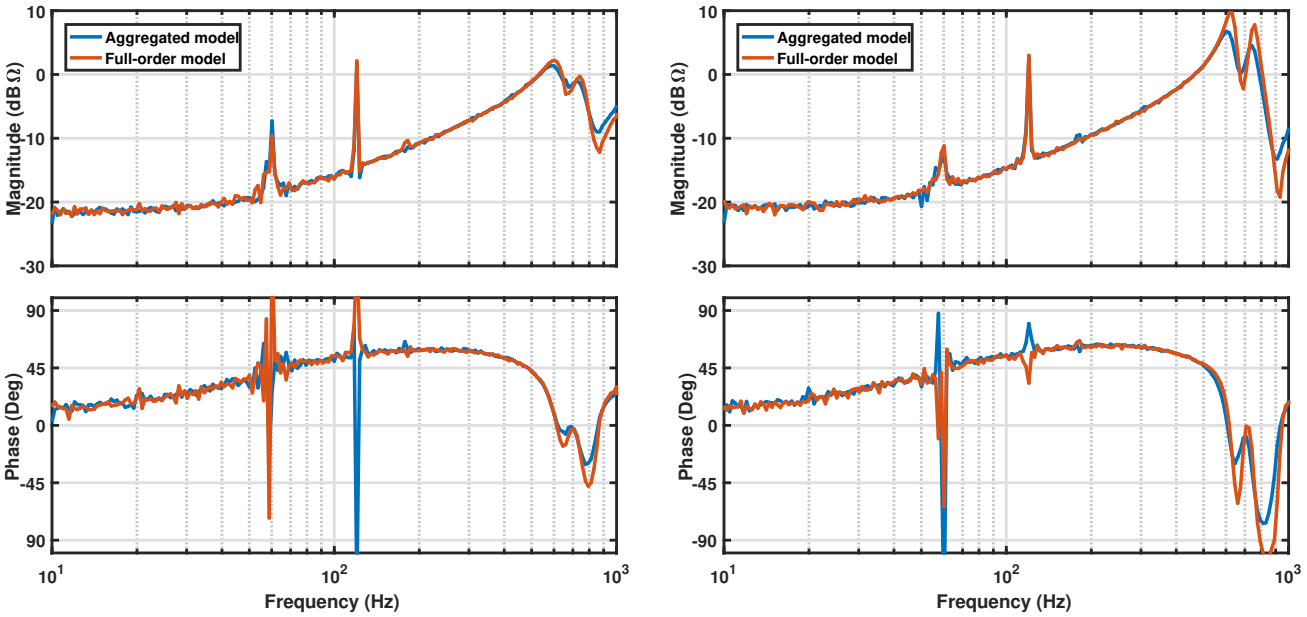


Fig. 9. Grid impedance measurements for high (left) and low (right) power consumptions.

and an LCL-filter connect the inverter to the grid emulator. A frequency-response analyzer (Venable FRA) is used to inject a sine-sweep current perturbation to grid through inverter control system. This causes a voltage perturbation and the ratio of the perturbations yields the grid impedance for each frequency. The impedance was measured from the q-channel ($Z_{\mathrm{qq}}$) with the output active power set to zero, in order to minimize the effects of harmonic currents, transformer saturation etc.

The cut-off frequency of the low-pass filter in current measurement for RTDS was set to 6 kHz to ensure interface stability. The loop gain of the grid emulation is given by

$$G = e^{-sT_{\mathrm{d}}}\, T_{\mathrm{a}}\, T_{\mathrm{f}} \tag{4}$$

where $e^{-sT_{\mathrm{d}}}$ is caused by total loop delay, $T_{\mathrm{a}}$ is amplifier transfer function, and $T_{\mathrm{f}}$ is low-pass filter transfer function, further given by

$$T_{\mathrm{a}} = \frac{e^{-3.7*10^{-6}s}}{3.57*10^{-12}s^2 + 2.70*10^{-6}s + 1} \tag{5}$$

$$T_{\mathrm{f}} = \frac{1}{25*10^{-6}s + 1} \tag{6}$$

as shown in [39]. Grid emulation transfer function $G$ does not affect magnitude below 1 kHz, but causes a significant phase drop. However, as the measurements from both models experience the same phase warp, the model comparison is not affected. Consequently, the transfer function can be compensated from the analytical expression for better comparability of analytical reference and measurement results, in order to verify the emulation model.

Fig. 10 presents the measured q-channel impedance and references for the aggregated model in high consumption state. When the phase drop caused by the PHIL setup shown in (4) is compensated, the measurement results are very accurate and follow well the compensated reference. Besides frequencies 60 and 120 Hz where the fundamental and second harmonic currents interfere and highly distort the results, the measurements have very low ripple and yield reliable results. At higher impedance values, the measurements are smoother as the perturbation becomes more significant, and thus easier to measure.

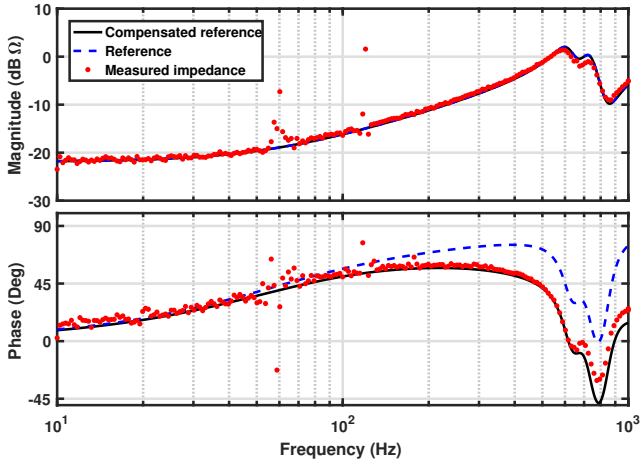


Fig. 10. Measured grid impedance $Z_{\mathrm{qq}}$ (red dots) in comparison with reference (dashed blue) and compensated reference (black).

The grid-impedance emulation of aggregated grid-impedance model is measured, and compared to the measurement from complex full-order model. The measurements are carried out for two different operation points of the simulated distribution system; first in low

consumption ($C_{\text{HH}} = 4.0$ $\mu$F, $P_{\text{HH}} = 400$ VA, $\text{PF}_{\text{HH}} = 0.9_{\text{ind}}$), and then in high-consumption scenario ($C_{\text{HH}} = 6.5$ $\mu$F, $P_{\text{HH}} = 2000$ VA, $\text{PF}_{\text{HH}} = 0.95_{\text{ind}}$). Fig. 9 shows the measured grid impedance q-components in high (left) and low consumption (right) for aggregated (blue) and full-order model (red).

The effectiveness of the model reduction method can be verified by comparing the results to the measurements from full-order model. Besides the resonant frequency around 700 Hz, the magnitude and phase are perfectly captured with the aggregated model. At resonant frequency, full-order model shows slightly reduced resonance damping and a few tens of Hz higher resonant frequency. This is mainly caused by the variation in household loadings and in transmission lengths to households in full-order model (both had $\pm 20\%$ variance), which was included to depict real conditions more accurately. The deviations in the resonant behavior are negligible and the measurement results are very similar for both scenarios. Thus, model reduction with aggregation of elements effectively replicates the results of the full-order model, yet model derivation is greatly simplified. Consequently, hardware requirements, computational burden, and modeling effort are drastically reduced.

## VI. Conclusion

The frequency-dependent grid impedance is an important parameter for stability assessment of grid-connected converters. A straightforward and commonly used RL-model is effective in suitable conditions; the model accurately captures the grid impedance in a simple grid-connection without nearby loads or capacitive grid elements. However, the method is often insufficient for modeling more complex grids. This work presents a method for aggregating grid elements of a complex multi-node system for simplified grid-impedance modeling. The hardware and computation requirements are drastically reduced as well as modeling effort, in comparison with detailed full-order model, while the impedance characteristics are still accurately replicated. Sensitivity analysis is carried out to illustrate the key components of the grid, and their impact on grid impedance.

Finally, the accuracy of the aggregated impedance model is verified by comparison with full-order model using experimental power hardware-in-the-loop setup. In the setup, a real 10 kVA three-phase inverter is used to measure the emulated grid impedance from a linear amplifier connected to real-time simulation. The measurements show very similar results for aggregated and full-order models. To conclude the work, the following suggestions are given for grid-impedance modeling; impact of loads should be considered, as well as the possibility of resonant behavior caused by the capacitive distribution system or capacitive grid elements. A simple and effective model can be derived from combination of upstream series RL-equivalent, aggregated consumer loads with equivalent capacitance, and transmission from the point-of-connection to the nearest node.

## Appendix

This appendix shows the derivation of dq-domain grid impedance from the state space presentation for a simple parallel RLC-circuit. The system can be represented as a state space

$$\begin{cases} \dot{\mathbf{x}} = \mathbf{A}\mathbf{x} + \mathbf{B}\mathbf{u} \\ \mathbf{y} = \mathbf{C}\mathbf{x} + \mathbf{D}\mathbf{u} \end{cases} \tag{7}$$

where states $\mathbf{x}$ are the voltages of capacitors and currents of inductors. Based on Kirchhoff's equations, the dq-transformed equations yield the following state matrices

$$\dot{\mathbf{x}} = \underbrace{\begin{bmatrix} -\frac{(AR_C+R_L)}{L} & \omega_s & \frac{A}{L} & 0 \\ -\omega_s & -\frac{(AR_C+R_L)}{L} & 0 & \frac{A}{L} \\ (\frac{AR_C}{RC} - \frac{1}{C}) & 0 & -\frac{A}{RC} & \omega_s \\ 0 & (\frac{AR_C}{RC} - \frac{1}{C}) & -\omega_s & -\frac{A}{RC} \end{bmatrix}}_{\mathbf{A}} \mathbf{x} + \underbrace{\begin{bmatrix} \frac{AR_C}{L} & 0 & -\frac{1}{L} & 0 \\ 0 & \frac{AR_C}{L} & 0 & -\frac{1}{L} \\ (\frac{1}{C} - \frac{AR_C}{RC}) & 0 & 0 & 0 \\ 0 & (\frac{1}{C} - \frac{AR_C}{RC}) & 0 & 0 \end{bmatrix}}_{\mathbf{B}} \mathbf{u} \tag{8}$$

$$\mathbf{y} = \underbrace{\begin{bmatrix} -AR_C & 0 & A & 0 \\ 0 & -AR_C & 0 & A \\ 1 & 0 & 0 & 0 \\ 0 & 1 & 0 & 0 \end{bmatrix}}_{\mathbf{C}} \mathbf{x} + \underbrace{\begin{bmatrix} AR_C & 0 & 0 & 0 \\ 0 & AR_C & 0 & 0 \\ 0 & 0 & 0 & 0 \\ 0 & 0 & 0 & 0 \end{bmatrix}}_{\mathbf{D}} \mathbf{u} \tag{9}$$

where $A = \frac{R}{R+R_C}$ and the dq-domain input, output, and state vectors are

$$\mathbf{u} = \begin{bmatrix} i_{ind} \\ i_{inq} \\ u_{od} \\ u_{oq} \end{bmatrix} \qquad \mathbf{y} = \begin{bmatrix} u_{ind} \\ u_{inq} \\ i_{od} \\ i_{oq} \end{bmatrix} \qquad \mathbf{x} = \begin{bmatrix} i_{Ld} \\ i_{Lq} \\ u_{Cd} \\ u_{Cq} \end{bmatrix}. \tag{10}$$

The frequency-domain transfer functions can be solved from the time-domain state space matrices 8 and 9 by using equation

$$\mathbf{Y}(s) = \big[\mathbf{C}(s\mathbf{I} - \mathbf{A})^{-1}\mathbf{B} + \mathbf{D}\big]\mathbf{U}(s) = \mathbf{G}\mathbf{U}(s) \tag{11}$$

where $s$ is the Laplace-variable, and $\mathbf{I}$ is the identity matrix. The transfer function matrix $\mathbf{G}$ is 4x4 matrix, where the transfer functions from current to voltage are the corresponding input impedances. Thus, the dq-domain input impedances can be extracted from $\mathbf{G}$

$$\underbrace{\begin{bmatrix} u_{ind} \\ u_{inq} \\ i_{od} \\ i_{oq} \end{bmatrix}}_{\mathbf{Y}(s)} = \underbrace{\begin{bmatrix} Z_{indd} & Z_{inqd} & \dots & \dots \\ Z_{indq} & Z_{inqq} & \dots & \dots \\ \dots & \dots & \dots & \dots \\ \dots & \dots & \dots & \dots \end{bmatrix}}_{\mathbf{G}} \underbrace{\begin{bmatrix} i_{ind} \\ i_{inq} \\ u_{od} \\ u_{oq} \end{bmatrix}}_{\mathbf{U}(s)}, \tag{12}$$

where the input impedances are the corresponding grid impedances as seen from inverter PCC.

## REFERENCES


[1] B. K. Bose, "Global energy scenario and impact of power electronics in 21st century," *IEEE Transactions on Industrial Electronics*, vol. 60, no. 7, pp. 2638–2651, July 2013.

[2] C. Li, "Unstable operation of photovoltaic inverter from field experiences," *IEEE Transactions on Power Delivery*, vol. 33, no. 2, pp. 1013–1015, 2018.

[3] C. Buchhagen, C. Rauscher, A. Menze, and J. Jung, "Borwin1 - first experiences with harmonic interactions in converter dominated grids," in *International ETG Congress 2015; Die Energiewende - Blueprints for the new energy age*, 2015, pp. 1–7.

[4] P. Belkin, "Event of 10-22-09," in *CREZ Technical Conference, Electric Reliability Council of Texas*, 2010.

[5] J. Sun, "Impedance-based stability criterion for grid-connected inverters," *IEEE Transactions on Power Electronics*, vol. 26, no. 11, pp. 3075–3078, 2011.

[6] S. L. Lorenzen, A. B. Nielsen, and L. Bede, "Control of a grid connected converter during weak grid conditions," in *2016 IEEE 7th International Symposium on Power Electronics for Distributed Generation Systems (PEDG)*, 2016, pp. 1–6.

[7] Q. Yang, K. Li, C.-M. Zhao, and H. Wang, "The resonance suppression for parallel photovoltaic grid-connected inverters in weak grid," *International Journal of Automation and Computing*, 05/24 2017. [Online]. Available: https://doi.org/10.1007/s11633-017-1072-0

[8] X. Chen, J. Chen, C. Gong, and H. Wang, "Impedance-based analysis of grid-connected inverter in high impedance grids," in *2013 IEEE 8th Conference on Industrial Electronics and Applications (ICIEA)*, 2013, pp. 1284–1289.

[9] A. Etxegarai, P. Eguia, E. Torres, A. Iturregi, and V. Valverde, "Review of grid connection requirements for generation assets in weak power grids," *Renewable and Sustainable Energy Reviews*, vol. 41, pp. 1501–1514, 2015.

[10] T. Midtsund, J. A. Suul, and T. Undeland, "Evaluation of current controller performance and stability for voltage source converters connected to a weak grid," in *The 2nd International Symposium on Power Electronics for Distributed Generation Systems*, 2010, pp. 382–388.

[11] J. Suul, S. D'Arco, P. Rodriquez, and M. Molinas, "Impedance-compensated grid synchronization for extending the stability range of weak grids with voltage source inverters," *IET Generation, Transmission & Distribution*, vol. 10, pp. 1315–1326, April 2016.

[12] J. Xu, B. Zhang, Q. Qian, X. Meng, and S. Xie, "Robust control and design based on impedance-based stability criterion for improving stability and harmonics rejection of inverters in weak grid," in *2017 IEEE Applied Power Electronics Conference and Exposition (APEC)*, 2017, pp. 3619–3624.

[13] D. Yang, X. Ruan, and H. Wu, "Impedance shaping of the grid-connected inverter with LCL filter to improve its adaptability to the weak grid condition," *IEEE Transactions on Power Electronics*, vol. 29, no. 11, pp. 5795–5805, 2014.

[14] J. Xu, S. Xie, and T. Tang, "Evaluations of current control in weak grid case for grid-connected lcl-filtered inverter," *IET Power Electronics*, vol. 6, no. 2, pp. 227–234, Feb 2013.

[15] M. Liserre, R. Teodorescu, and F. Blaabjerg, "Stability of photovoltaic and wind turbine grid-connected inverters for a large set of grid impedance values," *IEEE Transactions on Power Electronics*, vol. 21, no. 1, pp. 263–272, 2006.

[16] A. Knop and F. W. Fuchs, "High frequency grid impedance analysis by current injection," in *2009 35th Annual Conference of IEEE Industrial Electronics*, 2009, pp. 536–541.

[17] L. Jessen and F. W. Fuchs, "Modeling of inverter output impedance for stability analysis in combination with measured grid impedances," in *2015 IEEE 6th International Symposium on Power Electronics for Distributed Generation Systems (PEDG)*, 2015, pp. 1–7.

[18] S. Grunau, J. Reese, L. Jessen, and F. W. Fuchs, "Aspects of grid integration of renewable energy sources in weak power systems," in *International ETG-Congress 2013; Symposium 1: Security in Critical Infrastructures Today*, 2013, pp. 1–7.

[19] J. Xie, Y. Feng, and N. Krap, "Network impedance measurements for three-phase high-voltage power systems," in *Power and Energy Engineering Conference (APPEEC)*, 2010.

[20] L. Jessen and F. W. Fuchs, "Investigation of renewable energy generation and load impact on the grid impedance at different points of connection in public low voltage grids to support grid integration of renewable energies," *2016 18th European Conference on Power Electronics and Applications, EPE 2016 ECCE Europe*, 2016.

[21] J. H. R. Enslin and P. J. M. Heskes, "Harmonic interaction between a large number of distributed power inverters and the distribution network," *IEEE Transactions on Power Electronics*, vol. 19, no. 6, pp. 1586–1593, Nov. 2004.

[22] J. Meyer, R. Stiegler, P. Schegner, I. Röder, and A. Belger, "Harmonic resonances in residential low-voltage networks caused by consumer electronics," *CIRED - Open Access Proceedings Journal*, vol. 2017, no. 1, pp. 672–676, 2017.

[23] F. Barakou, M. H. J. Bollen, S. Mousavi-Gargari, O. Lennerhag, P. A. A. F. Wouters, and E. F. Steennis, "Impact of load modeling on the harmonic impedance seen from the transmission network," in *2016 17th International Conference on Harmonics and Quality of Power (ICHQP)*, Oct 2016, pp. 283–288.

[24] H. Alenius, "Modeling and electrical emulation of grid impedance for stability studies of grid-connected converters," 2018, Master's thesis, Tampere University of Technology.

[25] J. W. Feltes and B. S. Fernandes, "Wind turbine generator dynamic performance with weak transmission grids," in *2012 IEEE Power and Energy Society General Meeting*, 2012, pp. 1–7.

[26] N. Strachan and D. Dragan, "Stability of a variable speed permanent magnet wind generator with weak AC grids," *IEEE Transactions of Power Delivery*, 2010.

[27] L. D. Aguiar, R. Cardoso, C. Stein, P. D. Costa, and E. Carati, *Distributed Renewable Power Sources in Weak Grids - Analysis and Control*. Intechopen, 05/11 2016.

[28] D. Yang, X. Wang, F. Liu, K. Xin, Y. Liu, and F. Blaabjerg, "Adaptive reactive power control of PV power plants for improved power transfer capability under ultra-weak grid conditions," *IEEE Transactions on Smart Grid*, vol. PP, no. 99, pp. 1–1, 2017.

[29] X. Wang, D. Yang, and F. Blaabjerg, "Harmonic current control for LCL-filtered VSCs connected to ultra-weak grids," in *2017 IEEE Energy Conversion Congress and Exposition (ECCE)*, Oct 2017, pp. 1608–1614.

[30] M. Davari and Y. A. R. I. Mohamed, "Robust vector control of a very weak-grid-connected voltage-source converter considering the phase-locked loop dynamics," *IEEE Transactions on Power Electronics*, vol. 32, no. 2, pp. 977–994, Feb 2017.

[31] Y. Tang, L. Huang, and G. Zhao, "Resonant feed forward control for LCL-type grid-tied inverters in weak grid condition," in *2016 IEEE Energy Conversion Congress and Exposition (ECCE)*, 2016, pp. 1–6.

[32] Q. Zhao, H. Zhang, W. Song, X. Li, and Q. Yang, "Regulator reconstruction strategy of grid-connected inverter in weak grid," in *2016 IEEE 8th International Power Electronics and Motion Control Conference (IPEMC-ECCE Asia)*, 2016, pp. 451–457.

[33] J. J. Sun, W. Hu, H. Zhou, Y. M. Jiang, and X. M. Zha, "A resonant characteristics analysis and suppression strategy for multiple parallel grid-connected inverters with LCL filter," *Journal of power electronics*, vol. 16, pp. 1483–1493, 2016.

[34] R. Luhtala, T. Roinila, and T. Messo, "Implementation of Real-Time Impedance-Based Stability Assessment of Grid-Connected Systems Using MIMO-Identification Techniques," *IEEE Transactions on Industry Applications*, 2018.

[35] T. Roinila and T. Messo, "Online Grid-Impedance Measurement Using Ternary-Sequence Injection," *IEEE Transactions on Industry Applications*, 2018.

[36] T. Roinila, M. Vilkko, and J. Sun, "Broadband methods for online grid impedance measurement," in *2013 IEEE Energy Conversion Congress and Exposition*, Sept 2013, pp. 3003–3010.

[37] A. V. Timbus, R. Teodorescu, and P. Rodriguez, "Grid impedance identification based on active power variations and grid voltage control," in *2007 IEEE Industry Applications Annual Meeting*, 2007, pp. 949–954.

[38] S. Grunau and F. W. Fuchs, "Effect of wind-energy power injection into weak grids," in *European Wind Energy Conference and Exhibition 2012, EWEC 2012*, vol. 2, 2012, pp. 1150–1156.

[39] T. Reinikka, H. Alenius, T. Roinila, and T. Messo, "Power hardware-in-the-loop setup for stability studies of grid-connected power converters," in *IPEC-Niigata 2018 -ECCE ASIA*, 2018.